ADVANCED MATERIALS
www.advmat.de

Printing Green: Microalgae-Based Materials for 3D Printing with Light

*Clara Vazquez-Martel, Lilliana Florido Martins, Elisa Genthner, Carlos Almeida, Antera Martel Quintana, Martin Bastmeyer, Juan Luis Gómez Pinchetti, and Eva Blasco**

Microalgae have emerged as sustainable feedstocks due to their ability to fix CO_2 during cultivation, rapid growth rates, and capability to produce a wide variety of metabolites. Several microalgae accumulate lipids in high concentrations, especially triglycerides, along with lipid-soluble, photoactive pigments such as chlorophylls and derivatives. Microalgae-derived triglycerides contain longer fatty acid chains with more double bonds on average than vegetable oils, allowing a higher degree of post-functionalization. Consequently, they are especially suitable as precursors for materials that can be used in 3D printing with light. This work presents the use of microalgae as "biofactories" to generate materials that can be further 3D printed in high resolution. Two taxonomically different strains —*Odontella aurita* (*O. aurita*, BEA0921B) and *Tetraselmis striata* (*T. striata*, BEA1102B)— are identified as suitable microalgae for this purpose. The extracts obtained from the microalgae (mainly triglycerides with chlorophyll derivatives) are functionalized with photopolymerizable groups and used directly as printable materials (inks) without the need for additional photoinitiators. The fabrication of complex 3D microstructures with sub-micron resolution is demonstrated. Notably, the 3D printed materials show biocompatibility. These findings open new possibilities for the next generation of sustainable, biobased, and biocompatible materials with great potential in life science applications.

1. Introduction

Microalgae are photosynthetic unicellular microscopic organisms with extraordinary biodiversity. Under culture conditions, these microorganisms can be grown at different scales in fresh, salt, brackish and even wastewater without the need for arable land.[1–3] Microalgae fix atmospheric CO_2 while simultaneously producing biomass and O_2 during photosynthesis. Therefore, microalgae can be seen as efficient microscopic "biofactories" that are capable of producing a broad variety of interesting metabolites in a sustainable way.[4] Among these metabolites, lipids are of particular interest since they can be used as feedstock for new high-value materials. Microalgae are significantly more productive than conventional oil crops due to their considerable rapid growth rates and crop yields.[1,5] Thus, in the last decades, microalgae have already raised high interest in industry as a renewable source for fuel production as so-called third-generation biofuels that do not compete with human food production.[2,6] Microalgae have further been studied as microscopic biorefineries for olefins of different chain length[7] as well as for other high-added-value metabolites.[8] For example, microalgae-based oil has also been employed for the preparation of polyol architectures that can be converted into polyurethane foams.[9,10] Recently, microalgae have also been studied as environmentally friendly feedstocks for bioplastics, composites and even as "green" additives in construction materials such as cement.[11] For instance, whole spirulina cells were transformed into strong

C. Vazquez-Martel, L. Florido Martins, E. Blasco
Institute of Molecular Systems Engineering and Advanced Materials (IMSEAM)
Heidelberg University
Im Neuenheimer Feld 225, 69120 Heidelberg, Germany
E-mail: eva.blasco@oci.uni-heidelberg.de

The ORCID identification number(s) for the author(s) of this article can be found under https://doi.org/10.1002/adma.202402786

DOI: 10.1002/adma.202402786

E. Genthner, M. Bastmeyer
Zoological Institute
Cell and Neurobiology
Karlsruhe Institute of Technology (KIT)
Fritz-Haber-Weg 4
76131 Karlsruhe, Germany

C. Almeida, A. Martel Quintana, J. L. Gómez Pinchetti
Banco Español de Algas (BEA)
Universidad de Las Palmas de Gran Canaria (ULPGC)
Muelle de Taliarte s/n, Telde, Las Palmas 35214, Spain

M. Bastmeyer
Institute for Biological and Chemical Systems – Biological Information Processing (IBCS-BIP)
KIT
Hermann-von-Helmholtz-Platz 1, 76344 Eggenstein-Leopoldshafen, Germany

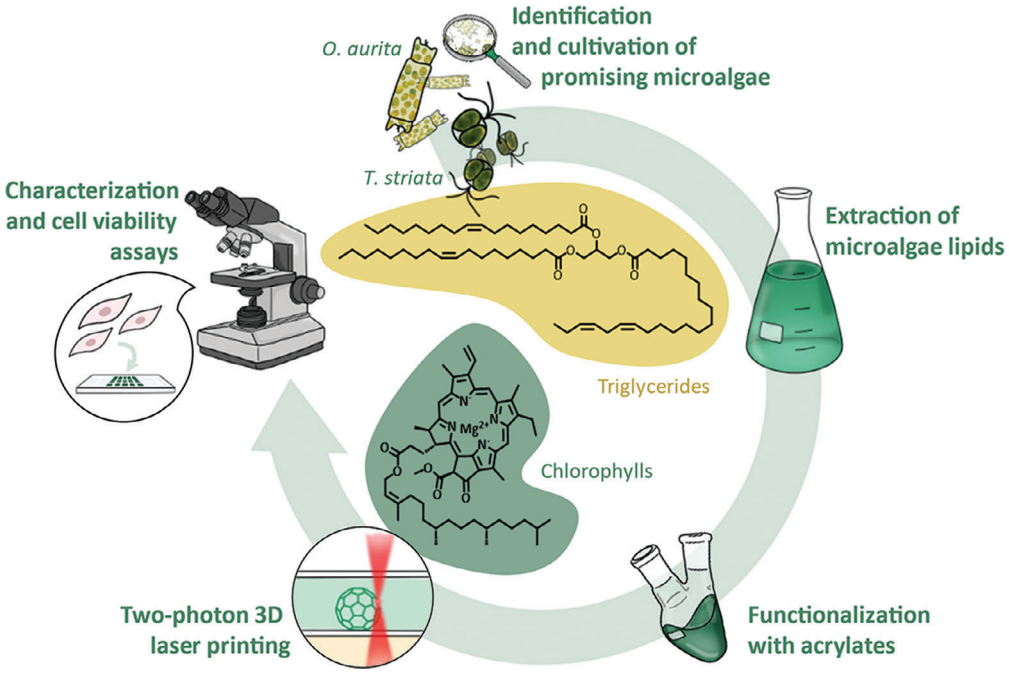

Figure 1. Overview of the approach established in this work. Two microalgae, namely *Odontella aurita* (*O. aurita*) and *Tetraselmis striata* (*T. striata*), have been selected and cultivated. The extracts obtained from these microalgae (mainly triglycerides with some chlorophylls) have been functionalized with photopolymerizable groups and used as printable materials for two-photon 3D laser printing. Furthermore, the 3D printed microstructures are afterwards characterized, and their biocompatibility is studied via cell viability assays.

and stiff compostable bioplastics employing a hot-pressing process without the need for additional binders or solvents.[12]

Additive manufacturing, also called 3D printing, allows for the fabrication of structures with complex geometries.[13] Algae, and microalgae in particular, are emerging as environmentally friendly materials for 3D printing at the macroscale using extrusion-based methods.[14] For example, 3D printing of microalgae-laden hydrogels has been demonstrated for applications in CO_2 capture or regenerative food.[15] Light-based 3D printing stands out among other additive manufacturing technologies due to its superior printing resolution and accuracy, surface quality and efficiency.[13,16,17] In particular, two-photon 3D laser printing has been established as an excellent method for manufacturing at the micro- and nanoscale. In brief, an infrared femtosecond laser is focused inside of a printable material —an ink— and induces non-linear multiphoton processes in its focal volume, also called voxel. Inside of this voxel, the laser intensity is sufficiently high to start curing of the ink locally, what allows for the creation of intricate 3D structures when scanning it within the ink. Due to its exceptional high resolution, it has become a key technology in a wide range of applications such as optics and photonics, microfluidics, bioengineering, and life sciences.[18,19,20] Conventional inks for two-photon 3D laser printing are composed of a mixture of (meth)acrylate monomers and crosslinkers, a photoinitiating system as well as other additives.[13,17,18] Most of the components of the inks are usually derived from petrochemicals contributing to the rapid depletion of fossil fuels and greenhouse gas emissions. Major efforts among the 3D printing community are being made towards the use of biomass-derived materials.[21] The main advantage of using bio-based materials relies both on their lower carbon footprint as well as their typically superior bio- and cytocompatibility.[20,22] So far, the main focus has been placed on the development of monomers and crosslinkers from renewable resources. For example, vegetable oils,[23,24] lignin and terpene-derivatives such as vanillin[25] and limonene,[26] diacids,[27] lactones,[28] and other aliphatic biomass,[29] have already been utilized as feedstock for light-based 3D printing. However, the usage of bio-based photoinitiating systems is still very limited.[30] The (cyto)toxicity of some photoinitiators represents a major burden, especially for biomedical applications.[20,31] Therefore, there is an urgent need for a broader palette of fully bio-based and biocompatible materials with disparate (physical and mechanical) properties that can be printed in high resolution with intricate topographies.

Herein, we present for the first time the use of microalgae as "biofactories" to generate materials that can be further used in high resolution 3D printing (**Figure 1**). In particular, two microalgae strains —*Odontella aurita* (BEA 0921B) and *Tetraselmis striata* (BEA 1102B)— with high content in lipids, mainly triglycerides, were selected and cultivated. The extracts were further functionalized and used as printing materials (inks). Interestingly, we also exploited the chlorophylls present in the extracts from the microalgae as photoactive system to induce polymerization without the necessity of adding a photoinitiating system. To the best of our knowledge, the use of chlorophylls for light-based 3D printing is entirely unprecedented. In the following step, we showcased the feasibility of manufacturing intricate 3D structures via two-photon 3D laser printing. The 3D printed structures were characterized in depth and their biocompatibility was studied via 3D cell viability assays.

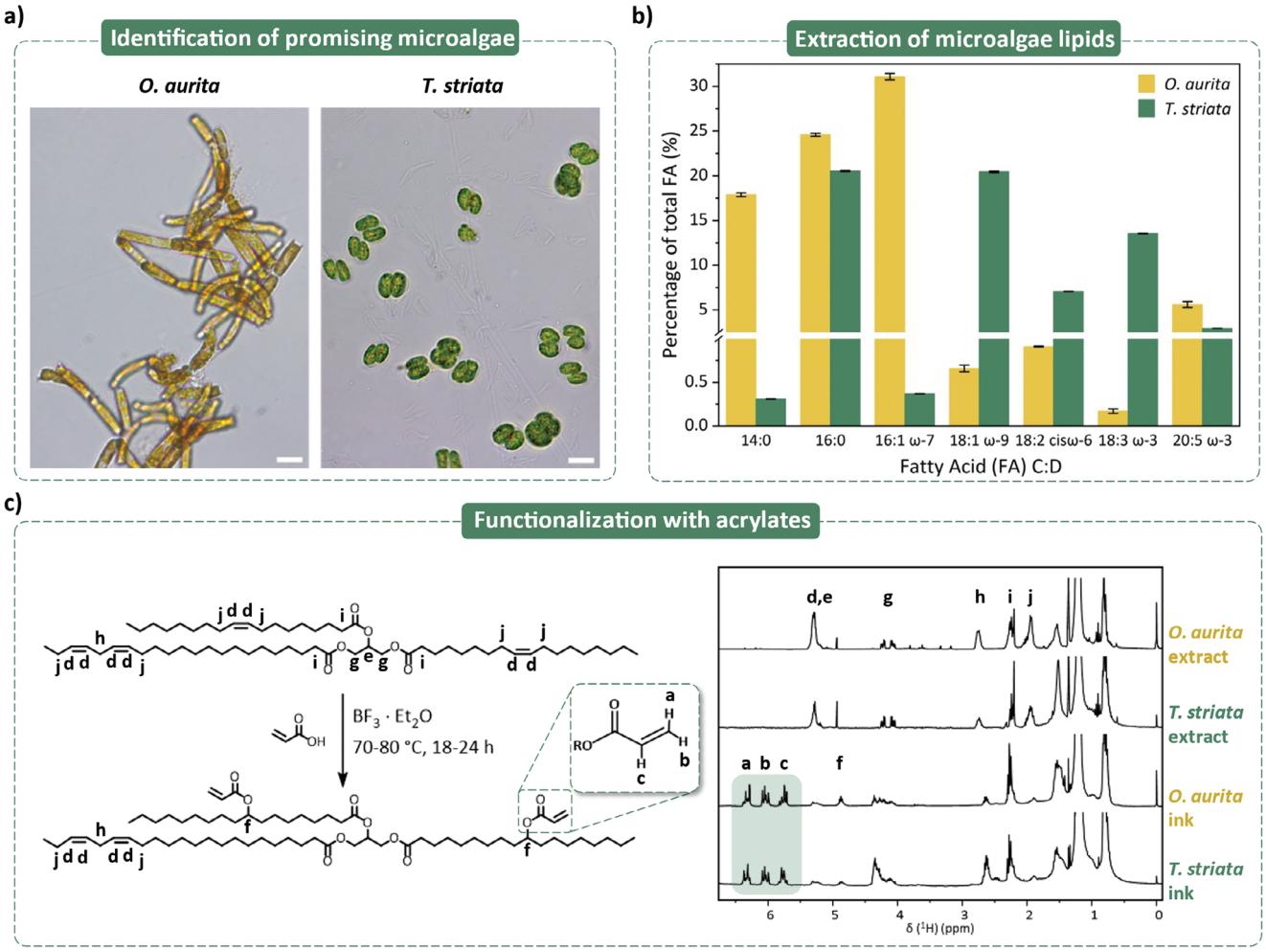

Figure 2. a) Light microscope images of the selected strains: *O. aurita* (left) and *T. striata* (right). Scale bar = 10 µm. b) Bar chart depicting the fatty acids methyl ester (FAME) profile of *O. aurita* and *T. striata*. Only the most relevant fatty acids are depicted (14:0, myristic acid; 16:0, palmitic acid; 16:1 ω−7, palmitoleic acid; 18:1 ω−9, oleic acid; 18:2 cis ω−6, linoleic acid; 18:3 ω−3, α-linolenic acid; 20:5 ω−3, eicosapentaenoic acid). For clarity, the y-axis has been segmented. c) Reaction scheme for the general functionalization reaction and ^{1}H-NMR spectra of the crude microalgae extracts before and after functionalization with acrylates (inks). Relevant protons for structural characterization have been assigned using the letters a-j.

2. Results and Discussion

2.1. Identification of Promising Microalgae for Extraction and Functionalization

For the present work, two taxonomically different strains from the *Culture Collection of the Spanish Bank of Algae* (BEA), *Odontella aurita* (*O. aurita*, BEA 0921B) and *Tetraselmis striata* (*T. striata*, BEA 1102B) have been selected (**Figure 2a**). *O. aurita* is a marine diatom (*Bacillariophyceae*),[32] while the genus *Tetraselmis* comprises well-known species that are members of the *Chlorodendrophyceae* family.[33] These strains were selected based on two main criteria: (1) high lipid (in particular, triglyceride) accumulation and (2) rapid growth rates and significant biomass production to enable upscaling (for further details on the cultivation of the strains please refer to the Experimental Section and to Figure S1, Supporting Information). As we have previously reported, the double bonds present in triglycerides (esters of glycerol and three fatty acids) enable easy chemical modification to introduce polymerizable groups, and consequently, becoming suitable materials for 3D printing with light.[23] It is worth noting that triglycerides derived from microalgae are composed of longer fatty acid chains with more unsaturations (= double bonds) on average than triglycerides derived from conventional oil crops such as sunflowers.[9] Therefore, it is expected that microalgae triglycerides are promising candidates as printable materials for two-photon laser 3D printing, where high degree of functionalization is crucial.[13] To demonstrate this, the type and unsaturation degree of the fatty acids accumulated in the two microalgae strains was monitored using gas chromatography with flame-ionization detection (GC–FID). The results obtained are summarized in Figure 2b (for further details please refer to Table S1, Supporting Information). Both strains contain lipids with high content of palmitic acid (C16:0). However, more interesting is the high values of palmitoleic acid (C16:1 ω−7) present in *O. aurita*, as well as the high concentration of oleic acid (C18:1 ω−9), linolenic acid (C18:2 cis ω−6) and α-linolenic acid (C18:3 ω−3, ALA) in *T. striata*. In addition, both strains contain moderate amounts of

polyunsaturated acids such as eicosapentanoic acid (C20:5 $\omega-3$, EPA). Although fatty acid profile strongly depends on the strain and the abiotic conditions,[32,34] the main fatty acids found in this study are in accordance with literature,[35] and importantly, prove the presence of unsaturated groups that are key for this study.

Once the high content of lipids in the cultivated microalgae was demonstrated and analyzed, a protocol for their extraction was optimized. Importantly, when extracting lipids from microalgae-based biomass, not only the microalgae strain selection is key but also the extraction method.[36,37] The latter ultimately depends on the targeted metabolite. In this work we aim for the extraction of the lipid fraction, preferably triglycerides, which can further be functionalized with photopolymerizable groups. Several considerations need to be taken into account to maximize the yield of the solvent extractions employed herein. While polar solvent mixtures, such as chloroform/methanol mixtures used in conventional lipid extraction protocols,[38,39] offer poor selectivity, non-polar solvents such as hexane are more suitable for the selective extraction of neutral lipids (i.e., hydrophobic and rather non-polar), and thus, triglycerides.[40] Therefore, hexane has been selected as the solvent of choice for the extraction procedure. Furthermore, cell wall disruption is needed in most cases to extract lipids effectively.[36] For this purpose, sonication and high-performance dispersing were employed as well. The presence of triglycerides in the extracts was confirmed using ^{1}H-NMR spectroscopy and thin layer chromatography (TLC) (Figure 2c, and Figures S2 and S3, Supporting Information). The *O. aurita-based* extracts contain triglycerides with 3.3 double bonds on average, while the double bond content is higher for the *T. striata-based* ones, with ≈4.6 double bonds per molecule. These results are in accordance with the lipid profiles presented previously.

The microalgae extracts were functionalized with acrylate groups adapting a previously reported solvent-free one-step approach (further details can be found in the Supporting Information).[23] The reaction was carried out for 24 h at a temperature of 75 °C and the double bond conversion was monitored by ^{1}H-NMR spectroscopy (Figure 2c, and Figures S4 and S5, Supporting Information). Please note that after functionalizing the microalgae-based extracts with acrylates they are referred to as "inks." Despite having a lower unsaturation degree (3.3), the *O. aurita-based* inks show high conversion of double bonds (68%), leading to 2.3 acrylate groups per molecule on average. *T. striata-based* inks exhibit a higher number of acrylate groups per molecule, with ≈2.8 and a double-bond conversion of 60%. The obtained values indicate that not only the quantity, but also the location of the unsaturations within the triglyceride molecule affects the conversion of double bonds (Figure S5, Supporting Information).[23]

2.2. Two-Photon Laser 3D Printing of Microalgae-Based Inks

The prepared microalgae-based inks contain between two and three acrylate groups per molecule, which is within the range of functionalization of common printable materials. Thus, the next step was to prove their suitability as printable materials. Along with the functional monomers/crosslinkers, one important component in the printing formulation is the photoinitiating system. The extracted triglycerides exhibit a dark green color due to the chlorophyll derivatives from the microalgae. These light sensitive species are present since they are highly lipid-soluble and thus are extracted along the triglycerides and remain after functionalization (Figure S6, Supporting Information). The concentration of these pigments can be estimated spectroscopically based on previous literature,[41] being 44 and 38 µg per 100 mg *O. aurita* ink and *T. striata* ink, respectively. These values correspond to ≈0.4 wt% photoinitiating species in the ink. Chlorophyll-removal, even in small quantities, is tedious and a common challenge in biofuel production.[42] However, in the context of this work, the presence of those chlorophylls residues can be beneficial for the printing process when used as a photoinitiating species. Thus, we investigate the possibility of using the functionalized extracts —without further purification— for two-photon 3D laser printing. Chlorophylls have been proven to be able to induce (controlled) radical photopolymerization of methacrylates and acrylamides.[41,43] Further, chlorophyll and their derivatives entail an aromatic porphyrin ring system which is known in the literature for its nonlinear optical properties.[44] Such processes are believed to play a central role in the complex electron transfer mechanisms during photosynthesis.[45] Thus, the microalgae-based inks rich in chlorophylls were tested in a commercial two-photon laser printer (Photonic Professional GT2 Nanoscribe GmbH & Co. KG, λ = 780 nm, **Figure 3a**). To prove the photopolymerization of the acrylate moieties initiated by chlorophylls during printing was successful, FTIR spectra of the microalgae-based extracts, inks and the 3D printed microstructures were recorded and compared (Figure 3b). It is clearly visible that the characteristic absorption bands attributed to the double bonds in the acrylate groups at 1636, 1620 and 809 cm^{-1} present in the ink decrease after 3D printing indicating their consumption during the printing process. A complete overview of the peaks and their assignment is provided in the Supporting Information (Figure S7 and Table S2, Supporting Information)

Next, the printability window was investigated by printing arrays of cylindrical pillars (diameter = 10 µm, z-height = 10 µm) with varying laser power intensity from 10 to 25 mW as well as varying laser scan speed from 6000 to 20 000 µm s^{-1}. The printed microstructures were characterized afterwards by scanning electron microscopy (SEM) imaging (Figure 3c). Both microalgae-based inks present similar printability windows (green labeling in Figure 3c). Too low energy doses (scan speeds above 14 000 µm s^{-1} at a laser power of 10 mW for *O. aurita-based* inks, and scan speeds above 18 000 µm s^{-1} at a laser power of 10 mW for *T. striata-based* inks) led to incomplete printing of the pillars due to poor network formation and low crosslinking degree.[46] However, if the energy dose is above a certain threshold (scan speeds below 8000 and 6000 µm s^{-1} at laser powers above 20 and 25 mW, respectively for *O. aurita-based* inks, and scan speeds below 12 000, 8000, and 6000 µm s^{-1} at laser powers above 15, 20, and 25 mW, respectively for *T. striata-based* inks), micro-explosions start to occur. The parameters that led to insufficient or not satisfactory printing quality are labelled in red and yellow, respectively, in Figure 3c. However, both microalgae-based inks present a broad printability window (green labeling in Figure 3c). In addition, the mechanical properties of the printed structures were determined by nanoindentation (Figure S8, Supporting Information). The structures printed with *O. aurita* inks exhibit a

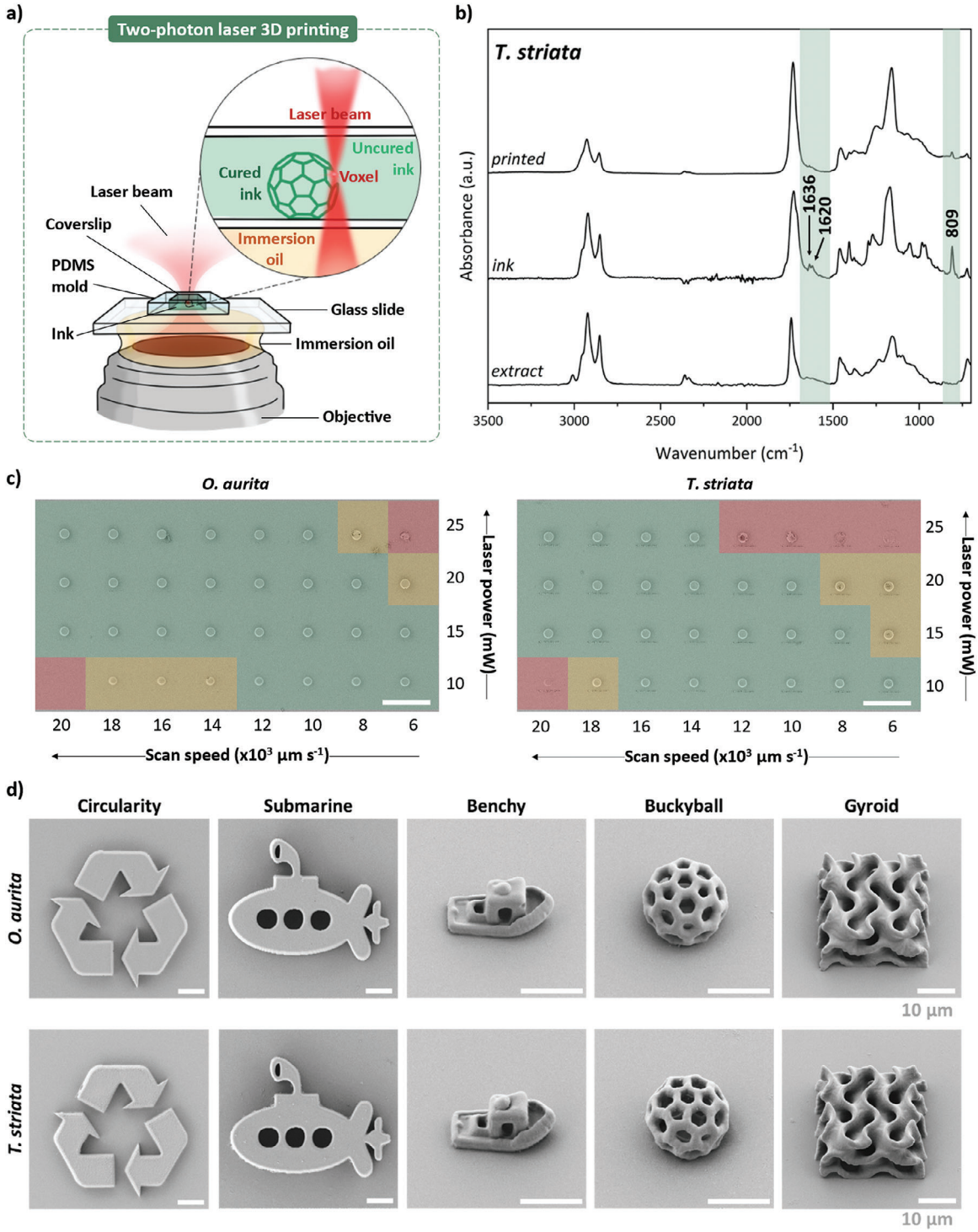

Figure 3. a) Schematic representation of the two-photon 3D laser printing setup employed in this work. b) FTIR spectra of *T. striata-based* extract, ink, and printed structures. c) SEM images of the dose test for printability window analysis of *O. aurita-based* and *T. striata-based* inks. Cylindrical pillars (z-height: 10 µm, Ø: 10 µm) were printed with varying laser power ranging from 10 to 25 mW in 5 mW steps, and the scan speed is varied from 6000 to 20 000 µm s^{-1} in 2000 µm s^{-1} steps. Green labeling stands for energy doses that yield successful prints, whereas the energy doses that result in structural failure of the pillars are labelled red; yellow labels intermediate results. Scale bar = 100 µm. d) SEM images of 3D microstructures printed using *O. aurita-based* and *T. striata-based* inks demonstrating the efficiency of the microalgae-based systems. In the case of *O. aurita-based* inks, a laser power of 25 mW and a scan speed of 12 000 µm s^{-1} were chosen for filigree structures such as the Benchy, the buckyball and the gyroid geometry. For bulky structures, such as the submarine and the circularity symbol, the scan speed was increased to 14 000 – 16 000 µm s^{-1}. For *T. striata-based* inks, laser powers between 15 and 20 mW at a scanning speed of 18 000 µm s^{-1} performed best for bulky structures, whereas filigree structures were preferably printed using 20 mW and 12 000 – 14 000 µm s^{-1}. Scale bar = 10 µm.

reduced elastic modulus of 108.7 ± 7.5 MPa and a hardness of 3.2 ± 0.1 MPa. In the case of the 3D microstructures printed using the *T. striata* ink, a higher modulus of 786.3 ± 51.6 MPa and a hardness of 31.5 ±1.5 MPa were measured.

To determine the minimum feature size and resolution of the developed materials, line patterns with different spacing (l_s) were printed with a laser power of 25 – 30 mW and a scanning speed of 200 – 250 µm s^{-1} (Figure S9, Supporting Information). *O. aurita-based* inks allow for a linewidth (l_w) of ≈750 – 770 nm, whereas *T. striata-based inks* permit thinner linewidths of 540 – 550 nm. It has been observed that the number of polymerizable groups per molecule affects the minimal feature size in a way that more polymerizable groups lead to a greater crosslinking density of the printed structures, hence allowing for thinner lines.[47] *T. strtata-based* inks have in average more acrylate groups per triglyceride (2.82) than the one from *O. aurita* (2.28), which would support this observation. The resolution, that is, the minimum distance between two lines that are still clearly separated, is similar for both microalgae-based inks, with 280 nm in the case of *O. aurita* and 330 nm for *T. striata*. Thus, sub-micron resolution using microalgae-based inks is demonstrated.

Once a suitable printing window was found and the limits in spatial resolution were determined, more complex 3D microstructures were printed to further prove the versatility of microalgae-based inks. Notably, both inks exhibited exceptional printing qualities (Figure 3d). A 2.5D "circularity" symbol (bounding box 50 × 50 µm, z-height: 5 µm) as well as a submarine (bounding box 60 × 50 µm, z-height: 10 µm) were first printed to demonstrate also that large, flat structures with very smooth surfaces can be printed. Then, the level of complexity of the structures was gradually increased by printing geometries that exhibited different degrees of overhanging features. The benchmark structure "Benchy" (small boat, bounding box 20 × 10 µm, z-height: 15 µm), was also successfully fabricated. This structure is specifically designed to provide a wide range of challenging geometrical features, such as the 90° overhang on the roof. Furthermore, a hollow fullerene buckyball structure (bounding box 15 × 15 µm, z-height: 15 µm) was successfully printed as well. In both cases it was possible to create free-standing structures with well-defined pentagons and hexagons. In the top-down view (Figure S10, Supporting Information) it is clearly visible, that the buckyballs are highly symmetrical and perfectly hollow. Finally, a porous, gyroid-like structure was printed (bounding box 30 × 30 µm, z-height: 17.5 µm). The pores of the structures are continuously open and well defined in both cases, as can be appreciated in the top-down view (Figure S10, Supporting Information). It should be noted that the optimal printing parameters were dependent on both the microalgae used and the geometry of choice. By using the optimized printing parameters, complex geometries with high quality were achieved for both inks.

2.3. Cell Viability Assays

To demonstrate the potential of the developed microalgae-based materials in bioapplications, several cellular assays were carried out (**Figure 4a**). First, the biocompatibility of the printed materials was investigated. Rat embryonic fibroblasts (REFs) were cultured on 5 × 5 arrays of 3D printed square scaffolds (bounding box 100 × 100 µm, z-height: 5 µm) in vitro for roughly 24 h (Figure 4b and Figure S11, Supporting Information). A LIVE/DEAD Viability/Cytotoxicity Kit was used to distinguish between living and dead cells. Living cells were stained with calcein-AM (λ_{ex} = 493 nm) and dead cells with ethidium homodimer-1 (EthD1) (λ_{ex} = 577 nm). In addition, the nuclei of cells were stained with Hoechst (λ_{ex} = 405 nm). The fluorescence images displayed in Figure 4b show that cells were distributed evenly on the surface as well as on the scaffolds while maintaining their viability for both microalgae-based materials. There was no significant difference in the cell viability of the two printed materials. Quantification of the Live/Dead assay using the JaCoP Plugin from ImageJ for colocalization analysis demonstrates that ≈99.8% of nuclei are in living cells labeled with calcein AM (Figure S12, Supporting Information). The absence of dead cells suggests that the microalgae-based materials have good cytocompatibility for fibroblasts. Furthermore, the reproducibility of the results was demonstrated by repeating the experiments three times (Figure S13, Supporting Information).

The immunostaining of the cells and the orthogonal projection in the YZ-direction display that the cells are well spread and located on top of the scaffolds (Figure S14a, Supporting Information). The position of the cell nuclei on top of the scaffolds is indicated by the white arrows. The orthogonal projection visualizes that the actin cytoskeleton is spanning across the whole scaffold. The scaffolds can be coated with fibronectin, which allows modification of the scaffolds with desired proteins for cell type-specific preference. Furthermore, the cell adhesion on the scaffolds surface is demonstrated by vinculin staining highlighting prominent focal adhesions (white arrows in Figure S14b, Supporting Information). In addition, proliferation activity of cells located on top of the scaffolds is verified by proliferation marker Ki-67 staining (Figure S14c, Supporting Information). Moreover, complex 3D scaffolds —namely a "wheel-like" scaffolds with overhanging bridges and micro-channels and a lattice scaffold with alternating rods— were successfully used for immunostaining experiments with REFs demonstrating potential applications for 3D culture conditions (Figure 4c,d).

3. Conclusions

In summary, we have demonstrated the use of microalgae as unique and sustainable "biofactories" for the development of biocompatible materials suitable for two-photon 3D laser printing. The two selected microalgae, *O. aurita* and *T. striata*, have been proved to be promising strains with high content in triglycerides. The extracted triglycerides were analyzed in terms of double bonds per molecule and subsequently functionalized by incorporating acrylate moieties as photoreactive units. Contrarily to state-of-the-art formulations, the novel approach presented herein relies on a bio-based and additive-free ink. Notably, the use of chlorophylls derivatives inherent in the microalgae extracts circumvents the issue of using non-bio-based and toxic photoinitiators or absorbers. The printability window, curing, resolution and minimal features have been thoroughly studied. It was possible to fabricate intricate and complex 3D geometries with different degrees of overhanging structures and sub-micron resolution. Furthermore, the biocompatibility of the printed microalgae-based structures was verified through cell viability studies. This

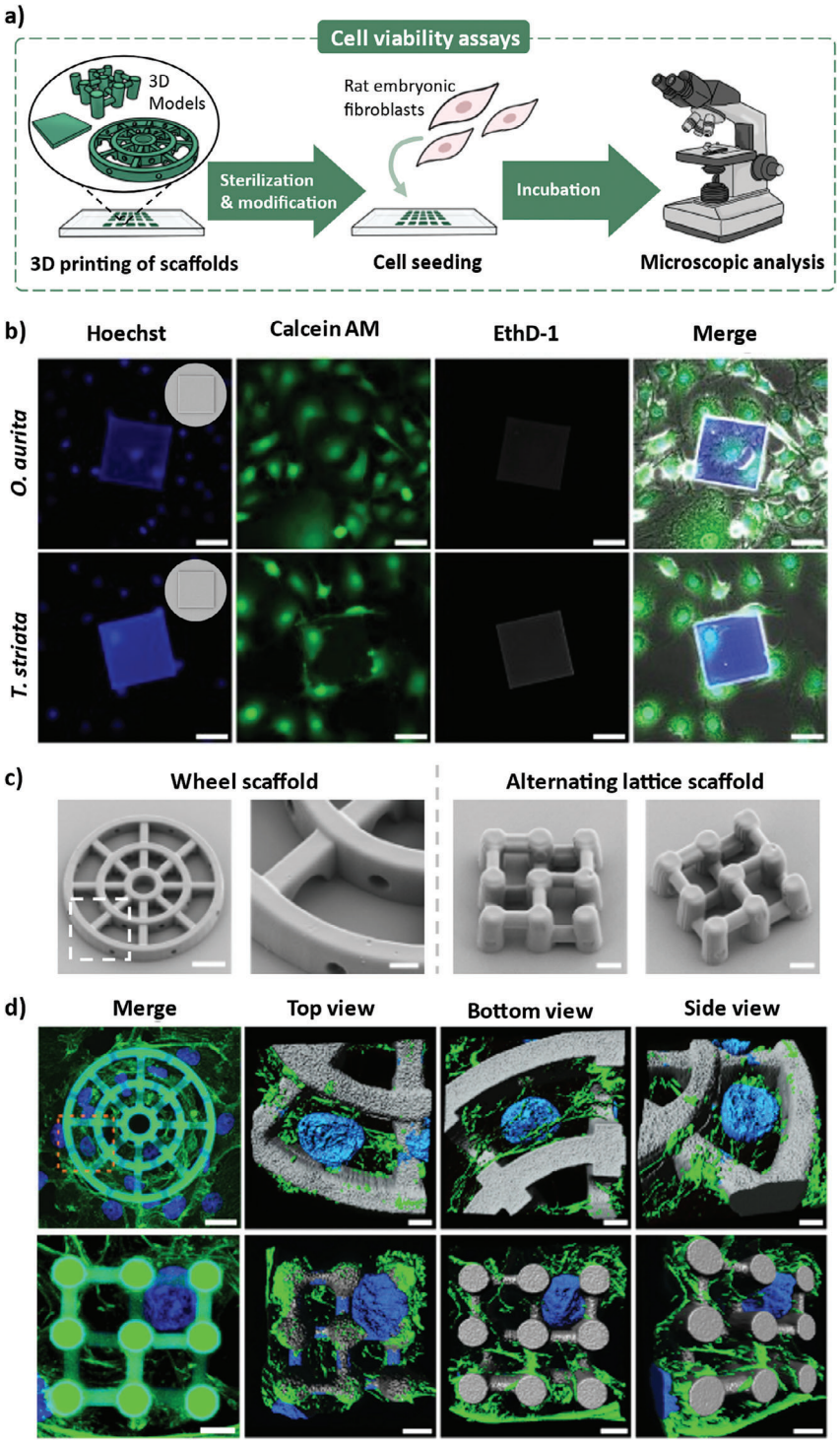

Figure 4. a) Different arrays of scaffolds are 3D printed, sterilized, and coated with fibronectin. Subsequently, rat embryonic fibroblasts (REFs) are seeded on top of the microstructures. After incubation the cell viability on the microstructures is studied. b) Fluorescence microscopy images of the live/dead assay of REF on printed *O. aurita* and *T. striata* 100 × 100 × 5 µm square microstructures. The inserts are SEM images of the microstructures. The excitation wavelength for the nuclei (Hoechst), alive cells (calcein AM) and dead cells (EthD-1) were 405 nm, 493 and 577 nm, respectively. The nuclei are depicted in blue, the live cells in green and the dead cells in red. Scale bar = 50 µm. c) SEM images depicting the two 3D scaffolds designed for the experiments. On the left, the big *"wheel"* scaffold with overhanging bridge structures and cylindrical channels is shown (Scale bar = 20 µm for the overview and 5 µm for the close-up section). On the right, a small lattice with alternating rods (Scale bar = 5 µm). d) Fluorescence microscopy images and 3D reconstruction using the microscopy image analysis software Imaris of REFs cultivated in the wheel-scaffold (top, scale bar = 20 µm for the merge overview and 5 µm for the close-up 3D reconstruction) and in the alternating lattice scaffold (bottom, scale bar = 5 µm). Nuclei are depicted in blue (DAPI), the actin cytoskeleton in green and the 3D reconstruction of the scaffold in grey (autofluorescence in 647 nm channel).

work highlights the vast potential of microalgae as a highly unexplored yet promising feedstock for two photon 3D laser printing. The usage of microalgae from two different taxonomic families also demonstrates the versatility of the presented approach. We believe that this work will facilitate advances in light-based 3D printing toward sustainable and functional bio-based materials, with potential applications as biocompatible implants or non-toxic 3D cell scaffolds.

4. Experimental Section

Materials: 2,6-di-tert-butyl-4-methylphenol (≥99.0%, Sigma Aldrich); 3-(trimethoxysilyl)propyl methacrylate (98%, Sigma Aldrich), acetic acid (100% p.A., Labochem); acrylic acid (98%, extra pure, stabilized, Acros Organics); boron trifluoride diethyl etherate ($BF_3{\cdot}Et_2O$, Sigma Aldrich); chloroform (≥99.8%, Fisher Chemical); chloroform-*d* (99.8 atom % D, Sigma-Aldrich); chlorophyll a (from spinach, Sigma Aldrich); diethyl ether (≥99.5%, Honeywell); glyceryl trioleate (≥99%, Sigma Aldrich); methyl sulfoxide (99.9%, for spectroscopy, Thermo Scientific); Na_2SO_4 (≥99%, Acros Organics); NaCl (99%, Honeywell Fluka); $NaHCO_3$ (99%, Grüssing GmbH); n-hexane (≥97.0%, Honeywell); oleic acid (90%, Sigma Aldrich); silica gel (technical grade, pore size 60 Å, 70–230 mesh, 63–200 µm); TLC silica gel 60 F_{254} (Supelco); toluene (≥99.5%, Honeywell) were used. Sylgard 184 PDMS (Dow) was purchased from Farnell. All materials were used as received without further purification unless otherwise stated. *Odontella aurita* (*O. aurita*, BEA 0931B) and *Tetraselmis striata* (*T. striata*, BEA 1102B) clonal strains were provided by the *Culture Collection of the Spanish Bank of Algae* (BEA).

Lipid Extraction: Lipids were extracted using a high-performance dispersing instrument (IKA T25 easy clean control ULTRA-TURRAX) at 12 000 rpm for 10 min.

^{1}H-NMR: Measurements of the samples in deuterated chloroform ($CDCl_3$) were performed using a Bruker Avance III 300 MHz equipped with a 5 mm BBO BB probe at 25 °C.

UV–Vis Measurements: UV–vis analysis was performed in DMSO using a Jasco V-770 Spectrophotometer and a 10 mm cuvette.

Fourier-Transform Infrared Spectroscopy: FTIR was conducted in the case of microalgae-based extracts and inks ("liquid" species) on a Jasco FT/IR-4600 FT-IR spectrometer in ATR mode with a resolution of 1 cm^{-1} and 32 scans. In the case of the 3D printed microstructures ("solid" species), infrared spectra were taken using Bruker LUMOS II FTIR microscope in ATR mode with a resolution of 4 cm^{-1} and 64 scans using a LN-MCT Mid detector (liquid N_2 cooled).

Light Microscopy: Microscopic images of the microalgae cells were recorded on a Leica DM6000B microscope with 40× magnification. The 3D printed microstructures were imaged on an Axio Imager M2 microscope (Carl Zeiss Microscopy) equipped with an LD Plan-Neofluar 20×/0.4 Korr Ph M27 objective and an Axiocam 705 microscope camera.

Scanning Electron Microscopy: SEM was performed using a field-emission scanning electron microscope (Ultra 55, Carl Zeiss Microscopy) at a primary electron energy of 3 keV. Prior to imaging, the 3D printed structures were sputter coated with a 12 nm layer of Pt/Pd (80:20).

Nanoindentation: The mechanical properties of the microalgae-based materials were characterized by nanoindentation on a Bruker Hysitron TI 980 Nanoindenter equipped with a low-load transducer and a diamond Berkovich tip. Prior to the measurements, the indentation tip was calibrated against air and the tip area function was calculated.

Fluorescence Microscopy: Experiments were performed with an LSM800 confocal microscope (Carl Zeiss Microscopy) equipped with a 40× oil immersion objective (NA = 1.4).

Microalgae Cultures and Growth Performance: Microalgae strains were cultured in f/2 medium[48] in 2L Erlenmeyer flasks under controlled conditions of light intensity (120.0 ± 10 µmol photons m^{-2} s^{-1}) and temperature (24 ± 1 °C). Cultures in triplicate were maintained under a 16:8 light/dark photoperiod and agitation was provided by filtered air (0.2 µm filtered). CO_2 pulses were injected at 15 s per hour during daylight periods. Cultures were inoculated at an optical density (OD) of 0.1 at 680 nm (Shimadzu UV-1900 UV–vis spectrophotometer) and growth was followed until the beginning of the stationary phase. At this point, cultures were harvested by centrifugation (Beckmann Coulter Avanti JXN-26 centrifuge), to start a new growth period from 0.1 OD in a semi-continuous mode. Biomass was harvested in different batches until at least 15 g of freeze-dried biomass (6.5 L Freeze dryer, Labconco, USA) was obtained. OD, temperature, and pH were measured every day except weekends. For further details, please refer to the Supporting Information.

Fatty Acid Profile by GC-FID: For fatty acid profile analysis, total lipids (TLs) were extracted from the microalgae according to the method described by Bligh and Dyer[39] with small modifications. The extractions were performed in triplicate. Fatty acids methyl esters (FAMEs) were obtained in triplicate by acid-catalyzed transmethylation of dry lipids extracts using 2 mL of 1% sulfuric acid in methanol and 1 mL of toluene to improve transmethylation of non-polar lipids. To avoid oxidation, the tubes were filled with N_2 gas, and then the reaction was performed at 50 °C for 16 h. After transmethylation, tubes were left at room temperature to cool down, and then 4 mL of hexane/diethyl ether (1:1 v/v) with BHT (0.01% w/v) and 2 mL of $KHCO_3$ (2% w/v) were added to each tube. The tubes were vortexed, and the hexane phase was recovered after centrifugation at 2000 rpm for 5 min at 4 °C. The aqueous phase was washed with 4 mL of hexane/diethyl ether, and after centrifugation the hexane phase was collected and combined to the previous organic phase to be dried under a stream of inert nitrogen. FAMEs were resuspended in hexane and filtered through a 0.45 µm filter prior injection. FAMEs were analyzed by a gas chromatograph equipped with a flame ionization detector (PerkinElmer Clarus 690 GC-FID) and a fused silica capillary column Elite-WAX (30m × 0.32 mm × 0.5 µm, PerkinElmer, Shelton, USA). Helium was used as carrier gas and column flow was held at 1.5 mL min^{-1}. Samples (1 µL) were injected in split mode (1:20) and the analysis parameters were: injector temperature at 240 °C and detector temperature at 250 °C. The initial column temperature was 50 °C for 1 min, before being increased to 150 °C at a rate of 40 °C min^{-1}, then increased to 200 °C at 2 °C min^{-1}, then to 214 °C at 1 °C min^{-1}, then to 230 °C at 40 °C min^{-1}, to a final temperature of 240 °C at 10 °C min^{-1} and held for 10 min. Nitrogen gas was used as make up gas (30 mL min^{-1}); flow of hydrogen gas and synthetic air were provided at 30 and 450 mL min^{-1}, respectively. FAMEs were identified by comparing their retention times with those of authentic standards (37 FAMEs, standard mixture, Supelco, Sigma-Aldrich). Nonadecanoic acid (C19:0) was used as internal standard. The relative quantification of FAMEs was calculated as percentage of the total FAs present in the analyzed microalgae. For further details, please refer to the Supporting Information.

Extraction of Microalgae Triglycerides: The lipid extraction procedure performed in this work was based on the method developed by Folch et al.[38] and was executed under yellow light conditions. Prior to extraction, 1.5 g of lyophilized biomass were placed in 30 mL hexane with 0.01% BHT (1:20 m/v) for 60 h and sonicated every 24 h for 60 min to disrupt the cell membranes and maximize lipid extraction yield. Next, the biomass was homogenized using a high-performance dispersing instrument (IKA T25 easy clean control ULTRA-TURRAX) at 12 000 rpm for 10 min in an ice bath. The homogenization step was repeated three times, and the extracts were then filtered. Then, 6 mL of a 0.88% KCl solution (5:1 v/v) were added to remove non-lipid contaminants. The aqueous phase was discarded, and the organic solvent was removed under reduced pressure. The desired extract was obtained as a viscous, dark green oil. Note that the hexane used for extraction can be collected and used for further extractions to avoid unnecessary organic solvent waste. The microalgae extracts were dissolved in chloroform and stored under nitrogen at −20 °C to avoid any hydrolysis and oxidation processes.

Functionalization with Acrylates: The functionalization reaction with acrylates of crude microalgae-based extracts from *O. aurita* and *T. striata* was adapted from the solvent-free, one-pot approach described in a previous work.[23] For further details, please refer to the Supporting Information.

Silanization: The substrates were treated to improve the adhesion of the 3D printed microstructures to the glass slide surface. For this purpose, glass coverslips (22 × 22 mm, 170 µm thickness) were washed with

isopropanol and acetone and dried under pressurized N_2. Then, the surface was cleaned and activated for 1.5 min by plasma treatment using a piezobrush PZ2 handheld plasma cleaner (Relyon Plasma GmbH, TDK Group Company). The coverslips were then immersed in a 4×10^{-3} M solution of 3-(trimethoxysilyl)propyl acrylate in toluene overnight. Finally, after washing twice in toluene and once in acetone, the silanized glass slides were used for printing.

Two-Photon 3D Laser Printing: 3D printing was performed on the commercially available setup Photonic Professional GT2 (Nanoscribe GmbH & Co. KG) in oil immersion configuration with a femtosecond laser (λ = 780 nm) focused through a 63× oil objective (NA = 1.4; WD = 190 µm; Zeiss). The instrument has a maximum output of 50 mW. The printing GWL files for 3D structure fabrication were generated from STL files of the desired geometries with the help of the Describe software (Nanoscribe). Slicing and hatching were set both to 300 nm. Printing was performed with laser powers in the range of 10 – 30 mW and scanning speeds between 200 – 20 000 µm s^{-1} depending on the desired structure. Silanized cover slides were attached by tape onto a commercial sample holder (Nanoscribe) for oil immersion mode. Immersion oil was added on the unfunctionalized slide surface, and the ink on the functionalized one to ensure good adhesion of the 3D printed microstructures. To maintain the environmental conditions of the ink as reproducible as possible, the ink was loaded into a PDMS mold and covered with a circular coverslip during printing. After printing, the PDMS mold was removed and uncured ink was removed. Different developing procedures were screened, including developing 10 min in hexane, 5 min in 1:1 acetone/isopropanol mixture and washing with water and soap as previously reported,[23] followed by drying. Employing water and soap yielded similar results to using organic solvents. 3D printing and the entire sample preparation and development were performed under yellow light conditions.

Nanoindentation Measurements: The measurements were performed at room temperature on 3D printed cylindrical pillars with 60 µm diameter. The printing parameters were kept constant for both microalgae, namely, a laser power of 20 mW and a scan speed of 14 000 µm s^{-1}. Nanoindentation was performed in load-controlled mode applying a trapezoid loading function with a loading and unloading rate of 50 µN s^{-1}, a peak force of 150 µN, and automatic drift control. For both microalgae, n = 5 measurements were performed, and a mean value and standard deviation were calculated. The reduced elastic modulus and the hardness values were calculated from the slope of the tangent of the elastic unloading curve according to literature.[49]

Cell Viability Assays and Immunocytochemistry: The tests were performed on 3D printed square scaffolds (bounding box 100 × 100 µm, z-height: 5 µm) fabricated by two-photon laser 3D printing with a laser power of 20 mW and a scanning speed of 14 000 µm s^{-1}. Arrays of 5 × 5 pedestals with 200 µm distance were prepared. Prior to cell culture, the cell scaffolds were sterilized with ultraviolet (UV) light for 30 min and coated with fibronectin (10 µg mL^{-1}) purchased from Sigma-Aldrich (St. Louis, MO, USA). Rat embryonic fibroblasts (REF) were seeded on the coated scaffolds using DMEM + 10% FCS from Pan-Biotech (Aidenbach, Germany) and incubated in a humidified incubator at 37 °C and 5% CO_2 overnight. To verify the cell viability, the LIVE/DEAD Viability/Cytotoxicity Kit from Invitrogen (Waltham, MA, USA) was used. The cells were labeled with calcein-AM or ethidium homodimer-1 (EthD1), for live or dead cells, respectively. The nuclei were stained with Hoechst 33 342 from Invitrogen. Incubation occurred for 30 min at 37 °C for all staining. The fluorescence images were observed using epifluorescence microscopy with a 5× or 20× objective lens. The excitation wavelengths were 401, 493, and 577 nm, respectively. For quantification of the cell viability, colocalization analysis using the JACoP plugin from ImageJ was performed. To exclude background signal, unspecific signal or autofluorescence of the resist, a threshold is set manually for the live/dead labeling and Hoechst staining to create binary images. To determine the cell nuclei, particles were analyzed to select regions of interest (ROI). The particle size was restricted to 5-infinity µm. Nuclei located on top of the scaffold were selected by drawing ROIs because of the autofluorescence of the photoresist. For the colocalization measurements, overlapping of the nuclei with the Calcein AM or EthD-1 channel was calculated. 3D Reconstructions of REFs cultivated in 3D scaffolds were compiled using the microscopy image analysis Software Imaris version 8.1.2.

Immunostaining was conducted to visualize the cell nuclei, actin filaments and fibronectin coating. Cells were fixed 24 h after seeding. The samples were incubated with anti-fibronectin (1:500), anti-Ki-67 (1:500) or anti-vinculin (1:100) in 1% (w/v) BSA in PBS, followed by washing with PBS (3 × 5 min) and incubation with a secondary antibody anti-rabbit AlexaFluor-488 (1:200), or anti-mouse AlexaFluor-488 in 1% (w/v) BSA in PBS. Incubation for both antibodies occurred for 1 h at room temperature in the dark. Nuclei and actin filaments were stained with DAPI (1:500) and Alexa Fluor 568 Phalloidin (1:200) during incubation of the secondary antibody.

Supporting Information

Supporting Information is available from the Wiley Online Library or from the author.

Acknowledgements

E.B. and M.B. acknowledge the funding from the Deutsche Forschungsgemeinschaft (DFG, German Research Foundation) via the Excellence Cluster "3D Matter Made to Order" (EXC-2082/1-390761711) and the Carl Zeiss Foundation through the "Carl-Zeiss-Foundation-Focus@HEiKA." C.V.M. acknowledges the Fonds der Chemischen Industrie for the financial support (Kekulé Fellowship). BEA-ULPGC thanks the support of the European Territorial Cooperation Program PCT-MAC 2014–2020 through the project REBECA-CCT (MAC2/1.1.B/269). The authors thank F. Kröger for his support during UV–vis measurements and S. Catt and P. Klee for their assistance during FTIR measurements. M. Taale is thanked for the fruitful discussions. In addition, R. Schröder, I. Wagner and R. Curticean are thanked for the access and training at the electron microscopy facilities.

Conflict of Interest

The authors declare no conflict of interest.

Data Availability Statement

The data that support the findings of this study are openly available in heiDATA, the Open Research Data institutional repository for Heidelberg University at https://doi.org/10.11588/data/KSMIGY.

Keywords

additive manufacturing, biocompatibility, microalgae, sustainability, two-photon polymerization

Received: February 23, 2024
Revised: June 5, 2024
Published online: June 22, 2024

[1] Y. Chisti, *Biotechnol. Adv.* **2007**, *25*, 294.
[2] L. Gouveia, A. C. Oliveira, *J. Ind. Microbiol. Biotechnol.* **2009**, *36*, 269.
[3] a) F. Wollmann, S. Dietze, J.-U. Ackermann, T. Bley, T. Walther, J. Steingroewer, F. Krujatz, *Eng. Life Sci.* **2019**, *19*, 860; b) F. L. Figueroa, N. Korbee, R. Abdala-Díaz, F. Álvarez-Gómez, J. L. Gómez-Pinchetti, F. G. Acién in *Bioassays. Advanced Methods and Applications*, (Eds.: D.-P. Häder, G. S. Erzinger), Elsevier, Amsterdam, **2018**.

[4] a) P. V. Sijil, C. Cherita, H. Jethani, V. S. Chauhan, in *Microalgae for Sustainable Products: The Green Synthetic Biology Platform*, (Eds.: A. Shekh, S. Dasgupta), The Royal Society of Chemistry, London **2022**; b) E. B. D'Alessandro, N. R. Antoniosi Filho, *Renewable Sustainable Energy Rev.* **2016**, *58*, 832.
[5] a) S. F. Ahmed, S. J. Rafa, A. Mehjabin, N. Tasannum, S. Ahmed, M. Mofijur, E. Lichtfouse, F. Almomani, I. A. Badruddin, S. Kamangar, *Energy Rep.* **2023**, *10*, 3297; b) M. M. A. Aziz, K. A. Kassim, Z. Shokravi, F. M. Jakarni, H. Y. Liu, N. Zaini, L. S. Tan, A. S. Islam, H. Shokravi, *Renewable Sustainable Energy Rev.* **2020**, *119*, 109621; c) C. F. Muñoz, C. Südfeld, M. I. S. Naduthodi, R. A. Weusthuis, M. J. Barbosa, R. H. Wijffels, S. D'Adamo, *Biotechnol. Adv.* **2021**, *52*, 107836; d) P. Singh, S. Kumari, A. Guldhe, R. Misra, I. Rawat, F. Bux, *Renewable Sustainable Energy Rev.* **2016**, *55*, 1.
[6] a) Q. Hu, M. Sommerfeld, E. Jarvis, M. Ghirardi, M. Posewitz, M. Seibert, A. Darzins, *Plant J.* **2008**, *54*, 621; b) F. Alam, A. Date, R. Rasjidin, S. Mobin, H. Moria, A. Baqui, *Procedia Eng.* **2012**, *49*, 221; c) C. Rösch, M. Roßmann, S. Weickert, *Global Change Biol. Bioenergy* **2019**, *11*, 326.
[7] a) J. Zimmerer, D. Pingen, S. K. Hess, T. Koengeter, S. Mecking, *Green Chem.* **2019**, *21*, 2428; b) N. S. Schunck, S. Mecking, *Angew. Chem., Int. Ed.* **2022**, *61*, 202211285; c) S. de Roo, F. Einsiedler, S. Mecking, *Angew. Chem., Int. Ed.* **2023**, *62*, 202219222.
[8] D. Liberti, P. Imbimbo, E. Giustino, L. D'Elia, G. Ferraro, A. Casillo, A. Illiano, G. Pinto, M. C. Di Meo, G. Alvarez-Rivera, M. M. Corsaro, A. Amoresano, A. Zarrelli, E. Ibáñez, A. Merlino, D. M. Monti, *ACS Sustainable Chem. Eng.* **2023**, *11*, 381.
[9] J. Peyrton, C. Chambaretaud, A. Sarbu, L. Avérous, *ACS Sustainable Chem. Eng.* **2020**, *8*, 12187.
[10] Z. S. Petrović, X. Wan, O. Bilić, A. Zlatanić, J. Hong, I. Javni, M. Ionescu, J. Milić, D. Degruson, *J. Am. Oil Chem. Soc.* **2013**, *90*, 1073.
[11] I. R. Campbell, M.-Y. Lin, H. Iyer, M. Parker, J. L. Fredricks, K. Liao, A. M. Jimenez, P. Grandgeorge, E. Roumeli, *Annu. Rev. Mater. Res.* **2023**, *53*, 81.
[12] H. Iyer, P. Grandgeorge, A. M. Jimenez, I. R. Campbell, M. Parker, M. Holden, M. Venkatesh, M. Nelsen, B. Nguyen, E. Roumeli, *Adv. Funct. Mater.* **2023**, *33*, 2302067.
[13] S. C. Ligon, R. Liska, J. Stampfl, M. Gurr, R. Mülhaupt, *Chem. Rev.* **2017**, *117*, 10212.
[14] a) S. Grira, H. A. Khalifeh, M. Alkhedher, M. Ramadan, *Int. J. Bioprint.* **2023**, *33*, e00291; b) S. Sayin, T. Kohlhaas, S. Veziroglu, E. Okudan, M. Naz, S. Schröder, E. I. Saygili, Y. Açil, F. Faupel, J. Wiltfang, O. C. Aktas, A. Gülses, *Mater. Today Chem.* **2020**, *17*, 100276; c) J. Foroughi, A. Ruhparwar, S. Aloko, C. H. Wang, *Macromol. Mater. Eng.* **2023**, *309*, 2300268; d) W. Sun, A. S. Williamson, R. Sukhnandan, C. Majidi, L. Yao, A. W. Feinberg, V. A. Webster-Wood, *Adv. Funct. Mater.* **2023**, *33*, 2303659.
[15] a) J.-J. Oh, S. Ammu, V. D. Vriend, R. Kieffer, F. H. Kleiner, S. Balasubramanian, E. Karana, K. Masania, M.-E. Aubin-Tam, *Adv. Mater.* **2024**, *36*, 2305505; b) S. Zhao, C. Guo, A. Kumarasena, F. G. Omenetto, D. L. Kaplan, *ACS Biomater. Sci. Eng.* **2019**, *5*, 4808; c) H. Liu, S. Yu, B. Liu, S. Xiang, M. Jiang, F. Yang, W. Tan, J. Zhou, M. Xiao, X. Li, J. J. Richardson, W. Lin, J. Zhou, *Adv. Mater.* **2024**, *36*, 2401172; d) S. Balasubramanian, K. Yu, A. S. Meyer, E. Karana, M.-E. Aubin-Tam, *Adv. Funct. Mater.* **2021**, *31*, 2011162.
[16] a) A. Bagheri, J. Jin, *ACS Appl Polym Mater* **2019**, *1*, 593; b) C. E. Cipriani, D. A. Dornbusch, S. L. Vivod, E. B. Pentzer, *RSC Appl. Polym.* **2024**, *2*, 71.
[17] G. A. Appuhamillage, N. Chartrain, V. Meenakshisundaram, K. D. Feller, C. B. Williams, T. E. Long, *Ind. Eng. Chem. Res.* **2019**, *58*, 15109.
[18] S. O'Halloran, A. Pandit, A. Heise, A. Kellett, *Adv. Sci.* **2022**, *10*, e2204072.
[19] a) P. Mainik, C. A. Spiegel, E. Blasco, *Adv. Mater.* **2023**, *36*, 2310100; b) D. Martella, S. Nocentini, D. Nuzhdin, C. Parmeggiani, D. S. Wiersma, *Adv. Mater.* **2017**, *29*, 1704047; c) S. Kawata, H. B. Sun, T. Tanaka, K. Takada, *Nature* **2001**, *412*, 697; d) S.-F. Liu, Z.-W. Hou, L. Lin, Z. Li, H.-B. Sun, *Adv. Funct. Mater.* **2023**, *33*, 2211280; e) G. von Freymann, A. Ledermann, M. Thiel, I. Staude, S. Essig, K. Busch, M. Wegener, *Adv. Funct. Mater.* **2010**, *20*, 1038; f) M. T. Raimondi, S. M. Eaton, M. M. Nava, M. Laganà, G. Cerullo, R. Osellame, *J. Appl. Biomater. Funct. Mater.* **2012**, *10*, 55; g) C. N. LaFratta, J. T. Fourkas, T. Baldacchini, R. A. Farrer, *Angew. Chem., Int. Ed.* **2007**, *46*, 6238.
[20] C. Greant, B. van Durme, J. van Hoorick, S. van Vlierberghe, *Adv. Funct. Mater.* **2023**, *33*, 2212641.
[21] a) E. Sanchez-Rexach, T. G. Johnston, C. Jehanno, H. Sardon, A. Nelson, *Chem. Mater.* **2020**, *32*, 7105; b) V. S. D. Voet, J. Guit, K. Loos, *Macromol. Rapid Commun.* **2021**, *42*, 2000475; c) E. M. Maines, M. K. Porwal, C. J. Ellison, T. M. Reineke, *Green Chem.* **2021**, *23*, 6863.
[22] a) T. Zink, R. Geyer, R. Startz, *J. Ind. Ecol.* **2018**, *22*, 314; b) J.-G. Rosenboom, R. Langer, G. Traverso, *Nat. Rev. Mater.* **2022**, *7*, 117; c) G. Hayes, M. Laurel, D. MacKinnon, T. Zhao, H. A. Houck, C. R. Becer, *Chem. Rev.* **2023**, *123*, 2609; d) V. Strehmel, B. Strehmel, *Appl. Res.* **2023**, *2*, 202300004.
[23] C. Vazquez-Martel, L. Becker, W. V. Liebig, P. Elsner, E. Blasco, *ACS Sustainable Chem. Eng.* **2021**, *9*, 16840.
[24] a) E. Skliutas, M. Lebedevaite, S. Kasetaite, S. Rekštytė, S. Lileikis, J. Ostrauskaite, M. Malinauskas, *Sci. Rep.* **2020**, *10*, 9758; b) B. Wu, A. Sufi, R. Ghosh Biswas, A. Hisatsune, V. Moxley-Paquette, P. Ning, R. Soong, A. P. Dicks, A. J. Simpson, *ACS Sustainable Chem. Eng.* **2020**, *8*, 1171.
[25] a) A. W. Bassett, A. E. Honnig, C. M. Breyta, I. C. Dunn, J. J. La Scala, J. F. Stanzione, *ACS Sustainable Chem. Eng.* **2020**, *8*, 5626; b) K. P. Cortés-Guzmán, A. R. Parikh, M. L. Sparacin, A. K. Remy, L. Adegoke, C. Chitrakar, M. Ecker, W. E. Voit, R. A. Smaldone, *ACS Sustainable Chem. Eng.* **2022**, *10*, 13091.
[26] E. Constant, O. King, A. C. Weems, *Biomacromolecules* **2022**, *23*, 2342.
[27] S. Pérocheau Arnaud, N. M. Malitowski, K. Meza Casamayor, T. Robert, *ACS Sustainable Chem. Eng.* **2021**, *9*, 17142.
[28] L. Yue, Y.-L. Su, M. Li, L. Yu, X. Sun, J. Cho, B. Brettmann, W. R. Gutekunst, R. Ramprasad, H. J. Qi, *Adv. Mater.* **2024**, 2310040.
[29] P. S. Klee, C. Vazquez-Martel, L. Florido Martins, E. Blasco, *ACS Appl. Polym. Mater.* **2024**, *6*, 935.
[30] a) C. Vazquez-Martel, P. Mainik, E. Blasco, *Organic Mater.* **2022**, *4*, 281; b) A. Al Mousawi, P. Garra, F. Dumur, B. Graff, J. P. Fouassier, J. Lalevée, *J. Polym. Sci.* **2020**, *58*, 254; c) A. Gallastegui, A. Dominguez-Alfaro, L. Lezama, N. Alegret, M. Prato, M. L. Gómez, D. Mecerreyes, *ACS Macro Lett.* **2022**, *11*, 303.
[31] a) G. Noirbent, F. Dumur, *Eur. Polym. J.* **2021**, *142*, 110109; b) J. L. Aparicio, M. Elizalde, *Packag. Technol. Sci.* **2015**, *28*, 181; c) F.-C. Bin, M. Guo, T. Li, Y.-C. Zheng, X.-Z. Dong, J. Liu, F. Jin, M.-L. Zheng, *Adv. Funct. Mater.* **2023**, *33*, 2300293.
[32] S. Xia, B. Gao, J. Fu, J. Xiong, C. Zhang, *J. Biosci. Bioeng.* **2018**, *126*, 723.
[33] a) M. F. Montero, M. Aristizábal, G. García Reina, *J. Appl. Phycol.* **2011**, *23*, 1053; b) H. Pereira, K. N. Gangadhar, P. S. C. Schulze, T. Santos, C. B. de Sousa, L. M. Schueler, L. Custódio, F. X. Malcata, L. Gouveia, J. C. S. Varela, L. Barreira, *Sci. Rep.* **2016**, *6*, 35663.
[34] I. Monteiro, L. M. Schüler, E. Santos, H. Pereira, P. S. Schulze, C. Florindo, J. Varela, L. Barreira, *Renewable Energy* **2023**, *208*, 693.
[35] a) T. Conde, S. Aveiro, T. Melo, T. Santos, B. Neves, P. Domingues, J. Varela, H. Pereira, M. R. Domingues, *Algal Res.* **2023**, *74*, 103218; b) F. Guihéneuf, M. Fouqueray, V. Mimouni, L. Ulmann, B. Jacquette, G. Tremblin, *J. Appl. Phycol.* **2010**, *22*, 629.
[36] J. B. Svenning, L. Dalheim, T. Vasskog, L. Matricon, B. Vang, R. L. Olsen, *Sci Rep* **2020**, *10*, 22229.
[37] P. Mercer, R. E. Armenta, *Eur. J. Lipid Sci. Technol.* **2011**, *113*, 539.

[38] J. Folch, M. Lees, G. H. Sloane Stanley, *J. Biol. Chem.* **1957**, *226*, 497.
[39] E. G. Bligh, W. J. Dyer, *Can. J. Biochem. Physiol.* **1959**, *37*, 911.
[40] a) M. Cooney, G. Young, N. Nagle, *Sep. Purif. Rev.* **2009**, *38*, 291; b) M. A. Danielewicz, L. A. Anderson, A. K. Franz, *J. Lipid Res.* **2011**, *52*, 2101; c) K. Ramluckan, K. G. Moodley, F. Bux, *Fuel* **2014**, *116*, 103; d) E. T. Yu, F. J. Zendejas, P. D. Lane, S. Gaucher, B. A. Simmons, T. W. Lane, *J. Appl. Phycol.* **2009**, *21*, 669.
[41] C. Wu, S. Shanmugam, J. Xu, J. Zhu, C. Boyer, *Chem. Commun.* **2017**, *53*, 12560.
[42] D. Y. Y. Tang, K. W. Chew, F. G. Gentili, C. Wang, H. S. H. Munawaroh, Z. Ma, F. Sun, M. Govarthanan, S. Alharthi, P. L. Show, *Ind. Eng. Chem. Res.* **2023**, *62*, 14478.
[43] a) N. Uri, *J. Am. Chem. Soc.* **1952**, *74*, 5808; b) S. Shanmugam, J. Xu, C. Boyer, *Chem. Sci.* **2015**, *6*, 1341; c) G.-X. Wang, J.-Y. He, L.-C. Liu, H. Wu, M. Zhong, *J. Polym. Res.* **2016**, *23*, 1023.
[44] J. A. N. Fisher, K. Susumu, M. J. Therien, A. G. Yodh, *J. Chem. Phys.* **2009**, *130*, 134506.
[45] A. R. Holzwarth, M. G. Müller, M. Reus, M. Nowaczyk, J. Sander, M. Rögner, *Proc. Natl. Acad. Sci. U.S.A.* **2006**, *103*, 6895.
[46] S. O. Catt, M. Hackner, J. P. Spatz, E. Blasco, *Small* **2023**, *19*, 2300844.
[47] D. Gräfe, A. Wickberg, M. M. Zieger, M. Wegener, E. Blasco, C. Barner-Kowollik, *Nat. Commun.* **2018**, *9*, 2788.
[48] R. R. Guillard, J. H. Ryther, *Can. J. Microbiol.* **1962**, *8*, 229.
[49] W. C. Oliver, G. M. Pharr, *J. Mater. Res.* **1992**, *7*, 1564.